Engineering Higgs dynamics by spectral singularities

H. P. Ojeda Collado [1,*], Nicolò Defenu [2], and José Lorenzana [1,†]

[1] *ISC-CNR and Department of Physics, Sapienza University of Rome, Piazzale Aldo Moro 2, I-00185, Rome, Italy*

[2] *Institute for Theoretical Physics, ETH Zurich, 8093 Zurich, Switzerland*

(Received 24 May 2022; revised 7 March 2023; accepted 8 March 2023; published 6 April 2023)

We generalize the dynamical phase diagram of a Bardeen-Cooper-Schrieffer condensate, considering attractive to repulsive, i.e., critical quenches (CQs) and a nonconstant density of states (DOS). We show that different synchronized Higgs dynamical phases can be stabilized, associated with singularities in the DOS and different quench protocols. In particular, the CQ can stabilize an overlooked high-frequency Higgs dynamical phase related to the upper edge of the fermionic band. For a compensated Dirac system we find a Dirac-Higgs mode associated with the cusp singularity at the Fermi level, and we show that synchronized phases become more pervasive across the phase diagram. The relevance of these remarkable phenomena and their realization in ensembles of fermionic cold atoms confined in optical lattices is also discussed.

DOI: 10.1103/PhysRevResearch.5.023011

I. INTRODUCTION

Many-body systems are characterized by the occurrence of correlated phenomena, which have no counterpart in the few-body realm. In this perspective, the spontaneous symmetry breaking (SSB) of any Hamiltonian symmetry by the establishment of a finite order parameter represents one of the fundamental examples [1–4]. Consequences of SSB include the appearance of superfluid and superconducting phases in condensed matter systems, as well as the occurrence of a finite mass of the intermediate vector bosons, the carrier particles of the weak force in the Standard Model [5–8].

The excitations on top of the SSB ground state, in systems with continuous (gauge) symmetries, consists of Nambu-Goldstone (phase) modes and massive Higgs (amplitude) modes. In the Standard Model, the latter manifest themselves as the Higgs boson, whose experimental observation led to the 2013 Nobel Prize in physics [9,10].

The historical tight relationship between condensed matter and high-energy physics is rooted in the universality of continuous SSB transitions, whose appearance in fermionic systems has been first described by the paradigmatic BCS theory [11,12]. Thus, it shall not surprise that Higgs mode dynamics has been observed across multiple systems in condensed matter, including superconductors with charge order [13–17], quantum antiferromagnets [18], and He^3 superfluids [19]. Its observation in superconducting systems [20–25] has been strongly debated [14–16,26–35].

Given the relevance and ubiquity of the Higgs mechanism, its observation was also the focus of quantum simulations in the superfluid/Mott-insulator transition of lattice bosons [36,37], in spinor Bose-Einstein condensates (BEC) [38] and in cavity-QED experiments [39]. A comprehensive picture of the Higgs mode features across the BEC-BCS crossover has recently been obtained in a fermionic cold atom ensemble [40], reinvigorating the interest of the cold atom's community in the signatures of SSB and Higgs mechanism also in the few-body limit [41,42].

Upon temporal variation of a control parameter, many-body dynamics may display several peculiar features, which are reminiscent of the behavior of thermodynamic functions at transition points [43]. In particular, theoretical investigations uncovered the appearance of dynamical phase transitions following interaction quenches in strongly correlated systems [44–49]. These dynamical transitions occur both as order parameter modulations and as singularities in the Löschmidt echo dynamics [50,51], which have been observed in quantum optics experiments [52,53]. These two phenomena have been shown to be deeply intertwined both between each other and with the existing equilibrium transitions [54,55], except for few examples [56–58].

Following the current perspective, we consider a critical quench (CQ) of the BCS model, i.e., an attractive to repulsive interaction quench where the sign of the coupling constant is flipped. Then, the system, which is prepared in the superconducting equilibrium state for attractive interaction, evolves according to a repulsive Hamiltonian, whose equilibrium ground state would be a normal (nonsuperconducting) gas. Due to the flexibility of our approach, we can target a wide range of different models parametrized by diverse density of states (DOS).

We find the distinctive features of the Higgs mode dynamics found in pioneering works [59,60], including synchronized oscillations of the order parameter. However, contrary to common belief, there is no a unique synchronized Higgs phase

*hector.pablo.ojedacollado@roma1.infn.it

†jose.lorenzana@cnr.it

(SHP) but different SHPs can be stabilized depending on the model and the protocol. The oscillation frequency can be determined by any spectral singularity. This includes those singularities not connected with the SSB but present in the bare DOS. Thus, a combination of protocol and the optical lattice in a cold atom system allows engineering generalized synchronized Higgs phases on demand.

II. MODEL

We consider a weak-coupling fermionic condensate with s-wave pairing described by the BCS model and subject to a sudden quench of the pairing interaction. The Hamiltonian can be written as

$$H_{\rm BCS} = \sum_{\boldsymbol{k},\sigma} \xi_{\boldsymbol{k}} \hat{c}^\dagger_{\boldsymbol{k}\sigma} \hat{c}_{\boldsymbol{k}\sigma} - \lambda(t) \sum_{\boldsymbol{k},\boldsymbol{k}'} \hat{c}^\dagger_{\boldsymbol{k}\uparrow} \hat{c}^\dagger_{-\boldsymbol{k}\downarrow} \hat{c}_{-\boldsymbol{k}'\downarrow} \hat{c}_{\boldsymbol{k}'\uparrow}, \tag{1}$$

where $\xi_{\boldsymbol{k}} = \varepsilon_{\boldsymbol{k}} - \mu$ measures the energy from the Fermi level μ and the pairing interaction $\lambda(t) = \lambda_i \theta(-t) + \lambda_f \theta(t)$ with θ the Heaviside step function. Here $\hat{c}^\dagger_{\boldsymbol{k}\sigma}$ ($\hat{c}_{\boldsymbol{k}\sigma}$) is the usual creation (annihilation) operator for fermions with momentum $\boldsymbol{k}$ and spin σ.

Due to the all-to-all interaction, a mean-field approach becomes exact in the thermodynamic limit. Thus, we shall consider the BCS mean-field Hamiltonian which can be written, using the Anderson pseudospin formulation [61] as

$$\hat{H}_{\rm MF} = -\sum_{\boldsymbol{k}} \hat{\boldsymbol{S}}_{\boldsymbol{k}} \cdot \boldsymbol{b}_{\boldsymbol{k}}. \tag{2}$$

Here $\boldsymbol{b}_{\boldsymbol{k}}(t) = (2\Delta(t), 0, 2\xi_{\boldsymbol{k}})$ represents an effective magnetic field vector for the $\frac{1}{2}$-pseudospin operator $\hat{\boldsymbol{S}}_{\boldsymbol{k}} = (\hat{S}^x_{\boldsymbol{k}}, \hat{S}^y_{\boldsymbol{k}}, \hat{S}^z_{\boldsymbol{k}})$ where

$$\begin{aligned}
\hat{S}^x_{\boldsymbol{k}} &= \frac{1}{2}(\hat{c}^\dagger_{\boldsymbol{k}\uparrow} \hat{c}^\dagger_{-\boldsymbol{k}\downarrow} + \hat{c}_{-\boldsymbol{k}\downarrow} \hat{c}_{\boldsymbol{k}\uparrow}),\\
\hat{S}^y_{\boldsymbol{k}} &= \frac{1}{2i}(\hat{c}^\dagger_{\boldsymbol{k}\uparrow} \hat{c}^\dagger_{-\boldsymbol{k}\downarrow} - \hat{c}_{-\boldsymbol{k}\downarrow} \hat{c}_{\boldsymbol{k}\uparrow}),\\
\hat{S}^z_{\boldsymbol{k}} &= \frac{1}{2}(1 - \hat{c}^\dagger_{\boldsymbol{k}\uparrow} \hat{c}_{\boldsymbol{k}\uparrow} - \hat{c}^\dagger_{-\boldsymbol{k}\downarrow} \hat{c}_{-\boldsymbol{k}\downarrow}).
\end{aligned} \tag{3}$$

Without loss of generality, we have assumed that the equilibrium BCS order parameter Δ is real, which remain true over time due to electron-hole symmetry. The instantaneous BCS order parameter is given by

$$\Delta(t) = \lambda(t) \sum_{\boldsymbol{k}} S^x_{\boldsymbol{k}}, \tag{4}$$

where symbols without a hat denote expectation value in the time-dependent BCS state. At equilibrium, the $\frac{1}{2}$-pseudospins align in the direction of their local fields $\boldsymbol{b}^i_{\boldsymbol{k}} = (2\Delta_i, 0, 2\xi_{\boldsymbol{k}})$ in order to minimize the system's energy.

The system is prepared with an initial interaction λ_i and a gap parameter satisfying the equilibrium gap equation,

$$1 = \lambda_i \int_{-W/2}^{+W/2} d\xi\, \rho(\xi) / \left(2\sqrt{\xi^2 + \Delta_i^2}\right), \tag{5}$$

where $\rho(\xi)$ is the DOS and the bandwidth satisfies, $W \gg \Delta_i$ ensuring the system is in the weak-coupling regime. The interaction is then suddenly changed to the final value, λ_f

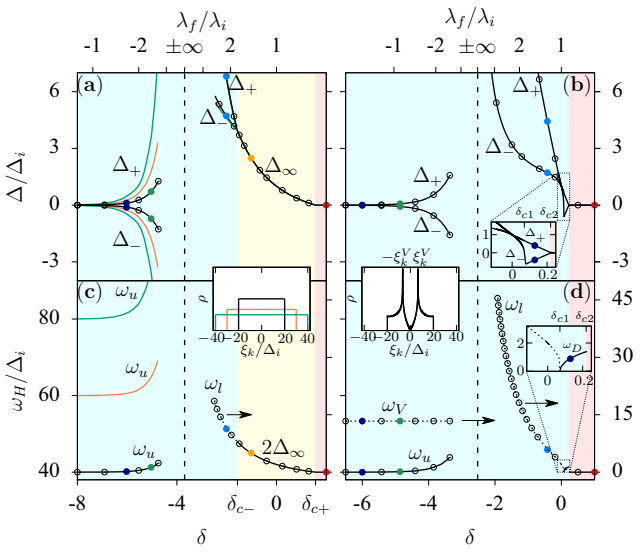

FIG. 1. Dynamical phase diagrams for the constant DOS (left) and the graphene-like DOS model (right) as schematized in the white background insets. The lower scale shows the control parameter δ. The vertical dashed line separates critical from noncritical quenches, while the upper scale is nonlinear and shows λ_f/λ_i for the particular case, $W = 40\Delta_i$. Panels (a) and (b) show extreme values of the order parameter characterizing the dynamics, while the lower panel shows the frequency of the Higgs oscillations labeled by the corresponding singularities in the quasiparticle DOS (see text). The background color indicates the different dynamical regimes: synchronized (magenta), damped oscillations (yellow), and overdamped (red). Full lines are obtained from the Lax root analysis, while circles are from numerical simulations (full circles correspond to dynamics shown in detail in other figures). The dashed line fitting the ω_l frequency is $2\bar{\Delta}$ from the simulations, which in panel (c) it converges to $2\Delta_\infty$ from the Lax root analysis. The dashed line fitting ω_V indicates $2\xi^V_{\boldsymbol{k}}$. Both ω_l and ω_V correspond to the right scale, as indicated by the arrows. The colored background insets are zoomed to the indicated regions. Arrows in (c) and (d) indicate data represented on the right-hand-side scale [62].

and the gap parameter is studied as a function of time. The pseudospins evolve according to

$$\frac{d\boldsymbol{S}_{\boldsymbol{k}}}{dt} = -\boldsymbol{b}_{\boldsymbol{k}}(t) \times \boldsymbol{S}_{\boldsymbol{k}} \tag{6}$$

($\hbar \equiv 1$) with the self-consistent order parameter $\Delta(t)$. We take $N = 10^4$ and 10^5 pseudospins within an energy range of $W = 40\Delta_i$, $60\Delta_i$ and $80\Delta_i$ around μ. We consider both a constant DOS and the DOS of a Dirac semimetal like graphene (see white background insets of Fig. 1). It is convenient to parametrize the quench by the variable

$$\delta \equiv \frac{W}{\lambda_f} - \frac{W}{\lambda_i}, \tag{7}$$

whose value is closely related to the one already used to parametrize noncritical quenches [60,63].

The out-of-equilibrium dynamics shows collective effects and single-particle (pseudospin) excitations. Similar to the case of periodic driving [64–68], we find that the latter are dominated by self-consistent pseudospin Larmor precessions

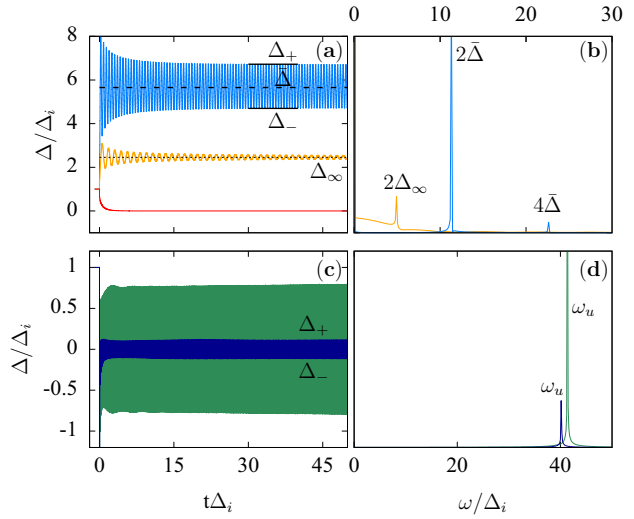

FIG. 2. Representative dynamics (left column) and their FT (right column) for the constant DOS case with $W = 40\Delta_i$. (a) Several traces of the superconducting order parameter, $\Delta(t)$, for quenches in the attractive side $\lambda_f/\lambda_f > 0$. The magenta curves correspond to a synchronized dynamics, while the orange and red ones correspond to a typical damped and overdamped dynamics, respectively. The FTs are shown in panel (b) where Higgs mode $2\bar{\Delta}$ and the second harmonic appear. The $2\Delta_\infty$ peak corresponds to a damped mode. (c) Two traces for CQ ($\lambda_f/\lambda_i < 0$) and their respective FTs in (d) showing a well-defined mode ω_u close to W. The quench parameters δ used in each case have been pointed out in Fig. 1 with colored dots. The FTs were computed considering a time window $t\Delta_i \in [5, 50]$.

encoding charge and pairing fluctuations. Their frequencies are given by $\Omega_L(\boldsymbol{k}) = 2E(\boldsymbol{k})$ where

$$E(\boldsymbol{k}) = \sqrt{\xi_{\boldsymbol{k}}^2 + \bar{\Delta}^2} \tag{8}$$

is the quasiparticle dispersion defined in terms of an average order parameter $\bar{\Delta}$ computed on a large time window after the quench. The familiar edge singularities in the quasiparticle DOS leads to analogous singularities in the DOS for Larmor fluctuations located at $2\bar{\Delta}$ and W ($\Delta \ll W$).

III. RESULTS

A. Dynamical phase diagram

Figure 1 shows the dynamical phase diagram for three different bandwidths and a constant DOS (left) and for the graphene-like DOS (right). Figures 1(a) and 1(b) show key values of the order parameter characterizing the dynamics, while Figs. 1(c) and 1(d) show the generalized SHP oscillation frequencies. Full lines were obtained exploiting the integrability of the model through a Lax roots analysis (see the Appendix for details) and were checked by numerical simulations (circles). The frequencies of Higgs modes are labeled according to a singularity of the quasiparticle DOS, namely, lower edge (l), upper edge (u), Van Hove (V), and Dirac point (D).

Figure 2 shows representative dynamics $\Delta(t)$ and their Fourier transform (FT) for the flat DOS case in each regime shown in the Fig. 1(a). The color of each curve matches the colored dots in Fig. 1(a) encoding the simulation parameters. Figures 2(a) and 2(b) correspond to noncritical quenches $\lambda_f/\lambda_i > 0$, while Figs. 2(c) and 2(d) correspond to the CQ.

The curves to the right of the vertical dashed line in Figs. 1(a) and 1(c) reproduce the results of Ref. [60] where three dynamical phases were found for noncritical quenches $\lambda_f/\lambda_i > 0$. In the top panels of Fig. 2, we can see examples of these behaviors: persistent oscillations (blue), damped oscillations (orange) and overdamped dynamics (red). The former corresponds to the lower-edge Higgs mode with frequency $\omega_l = 2\bar{\Delta}$ as can be seen in Fig. 2(b) where also a second harmonic peak at $4\bar{\Delta}$ appears. In the damped regime, a peak at frequency $2\Delta_\infty$ is also resolved due to the finite time window we consider computing the FT.

Coming back to the dynamical phase diagram in Figs. 1(a) and 1(c) for a small increase or decrease of the attractive interaction (small $|\delta|$), the superconducting order parameter shows damped oscillations with a Higgs frequency associated with the lower edge of the quasiparticle DOS, $\omega_l = 2\Delta_\infty$. Then it saturates to a constant value Δ_∞ at long times, which therefore coincides with $\bar{\Delta}$ (yellow shading in Fig. 1). For large quenches, there are two possible outcomes. Decreasing the pairing constant beyond a critical point ($\delta > \delta_{c+} = \pi/2$), the system goes to the gapless regime ($\Delta_\infty = 0$) with an overdamped dynamics (red region). Increasing the pairing above a critical point ($\delta < \delta_{c-} = -\pi/2$), the system synchronizes and the order parameter oscillates between the values Δ_+ and Δ_- with a fundamental Higgs frequency equal to twice the average order parameter [69], $\omega_l = 2\bar{\Delta}$ (magenta area). We will refer to this well known phenomena [59,60,63] as the "lower-edge SHP."

Using δ as the control parameter has the advantage that for large enough bandwidth, the results for $\lambda_f/\lambda_i > 0$ become independent of the bandwidth, so the curves for different W fall almost on top of each other.

The region to the left of the vertical dashed line shows the result of the CQ. A different synchronized regime is found where the order parameter oscillates with *symmetric* amplitudes Δ_+ and Δ_- around zero instead of having a finite average $\bar{\Delta}$. Two representative dynamics of this phase and their FTs are shown in Figs. 2(c) and 2(d). This zero-order-parameter average (ZOPA) behavior is reminiscent of the time-crystal phases found with periodic driving [65,66]. In contrast to the purely attractive interaction quench, the amplitudes and the Higgs frequency are strongly dependent on the bandwidth (compare the left part of Figs. 1(a) and 1(c) with the right part). In this case, the SHP frequency converges to the upper edge of the fluctuation DOS ($\omega_u \to W$), when the final interaction is repulsive and small (large negative δ) [see Fig. 1(c) and Fig. 2(d)]. For $\delta < -8$ (small repulsive λ_f) the amplitude becomes vanishing small and the dynamical phase can not be distinguished from a gapless state. Therefore, for large negative and positive δ ($\lambda_f \to \pm 0$) the system converges to the same gapless phase.

The occurrence of SHP associated with upper and lower edges of the fluctuation/quasiparticle DOS suggests that singularities act as a nucleation centers in frequency space to stabilize the synchronized phases during the nonlinear dynamics. We expect this mechanism to be ubiquitous, thus leading to the appearance of Higgs mode signatures in any

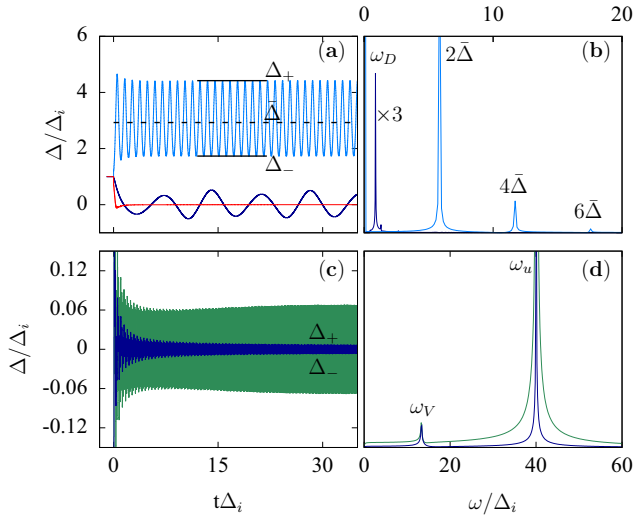

FIG. 3. Same as Fig. 2 for the graphene-like DOS case. For the noncritical quenches (a), the magenta and dark-blue curves correspond to synchronized phases, while we show in red a typical dynamics in the overdamped regime. Notice that the FT in (b) shows peaks related to Higgs mode $2\bar{\Delta}$ and high harmonics, as well as ω_D. In (d), in addition to the strong response with frequency $\omega_u \simeq W$, also a frequency ω_V emerges. This Higgs mode is related to the Van Hove singularities in the graphene-like DOS (see text). The time window is as in Fig. 2 except to resolve the slow Dirac-Higgs mode [dark blue curves in panels (a) and (b)] for which we use $t\Delta_i \in [5, 300]$ [62].

BCS system with singular DOS. In order to confirm this expectation, we have studied the dynamical phase diagram of a Dirac system with a graphene-like DOS where two additional singularities are present already in the bare DOS: one at the Fermi level (Dirac point) and the Van Hove singularities at $\xi_{\boldsymbol{k}}^V \approx \pm 6.66\Delta_i$ (see DOS in the white background inset of right panels of Fig. 1).

Interestingly, the phase diagram of the graphene-like model turns out to be quite different from the flat-DOS case. The damped regime (yellow region) is completely absent and synchronization occurs even for an *arbitrary small* quench [see zoomed region inset in Fig. 1(b)]. A hint of this behavior can be obtained from linear response theory [70]. The imaginary part of the susceptibility shows a sharper and more intense Higgs mode in the case of the Dirac system, indicating less propensity to decoherence than the flat-DOS case. One arrives to the same conclusion studying the participation ratio of quasiparticles to the Higgs mode and the phase diagram of related models with an indentation in the DOS near the Fermi level (Sec. III C).

Also, differently from the constant DOS model, the synchronization phenomenon takes place for both an increase and a decrease of the pairing interaction. In the latter case, decreasing enough λ_f, the pseudospins effectively decouple from each other and the gapless regime is recovered (red region). A representative dynamics of this phase is shown in Fig. 3(a) in red using the parameters indicated with a red circle in Fig. 1(b).

Between the $\delta = 0$ and the overdamped gapless phase, a quite rich transition is found, as shown in the zoomed insets of Figs. 1(b) and 1(d). First, twice the average order parameter (thin dashed line) and the frequency ω_l decrease very rapidly tracking each other, as in other non-ZOPA synchronized phases, until a critical value $\delta_{c1} = 0.07$ where both are driven to zero. Beyond this δ_{c1}, a ZOPA synchronized phase appears associated to the Dirac point singularity with a frequency ω_D as shown in dark blue in Figs. 3(a) and 3(b). This dynamical phase is stable in a very narrow window of the phase diagram with the frequency ω_D increasing with δ until it collapses in the overdamped phase at a second critical value $\delta_{c2} = 0.22$.

The FT of the dynamics shown in Fig. 3(b) reveals that in the lower-edge SHP, the graphene-like model shows up to three harmonics while in the flat DOS model only two harmonics are visible for the present parameters [Fig. 2(b)]. The synchronized Dirac-Higgs phase, in contrast, appears much more harmonic.

Figure 3(c) and 3(d) exemplify the dynamics for the CQ corresponding to the matching color full dots in Figs. 1(b) and 1(d), where the upper-edge SHP is excited. The overall appearance is very similar to the case of a flat DOS [Figs. 2(c) and 2(d)] showing ZOPA behavior. However, an extra weak modulation appears, which is revealed as a new frequency ω_V in the Fourier transform [Fig. 3(d)]. This frequency matches twice the Van Hove singularity in the DOS $2\xi_{\boldsymbol{k}}^V$, thus as expected, a synchronized Van Hove–Higgs mode can be excited. Its amplitude decreases in time, indicating that the mode is damped, although with quite a long coherence time, as witnessed by the narrow peak in the FT.

To fully characterizes the dynamical phases and the emergence of synchronization in the system, it is instructive to analyze the $\xi_{\boldsymbol{k}}$-resolved FT of the pseudospin dynamics. As we are interested in the pairing dynamics, we show the FTs of the x component of pseudospins for the flat DOS model and the graphene-like model in Figs. 4 and 5, respectively. In these figures, single-particle (pseudospin) excitations appear as dispersive features, while synchronized collective modes appear as vertical lines.

Figures 4(a) and 5(a) show the pseudospin-resolved FT of the dynamics in the lower-edge SHP with $\lambda_f/\lambda_i > 0$, for the flat-DOS and the graphene-like DOS case respectively. The large black dots correspond to the Larmor frequency $\Omega_L = 2\sqrt{\xi_{\boldsymbol{k}}^2 + \bar{\Delta}^2}$. In addition, of the main $\Omega_L(\boldsymbol{k})$ dispersion, Floquet side bands appear analogous to the bands observed under periodic drive [65,71]. Here, of course, an external periodic drive is not present and the bands are self-generated by the action of the lower-edge Higgs mode with frequency ω_l yielding replicas (small black dots) at $\Omega_L(\boldsymbol{k}) + n\omega_l$ with $n = -1, 0, 1, 2, \ldots$ and weaker features at $-\Omega_L(\boldsymbol{k}) + n\omega_l$ with $n = 0, 1$. The same panels show that the lower edge Higgs mode is not determined only by the quasiparticles participating in the edge singularity of $\Omega_L(\boldsymbol{k})$ at the frequency $2\bar{\Delta}$. Indeed, the vertical feature emerging from $2\bar{\Delta}$ witnesses that all quasiparticles in this $\xi_{\boldsymbol{k}}$ window are synchronized and participate in the collective mode. Thus, the edge singularity of the dispersion can be seen as a nucleation center in frequency space given a "rhythm" which is followed by the rest of the quasiparticles due to the interactions.

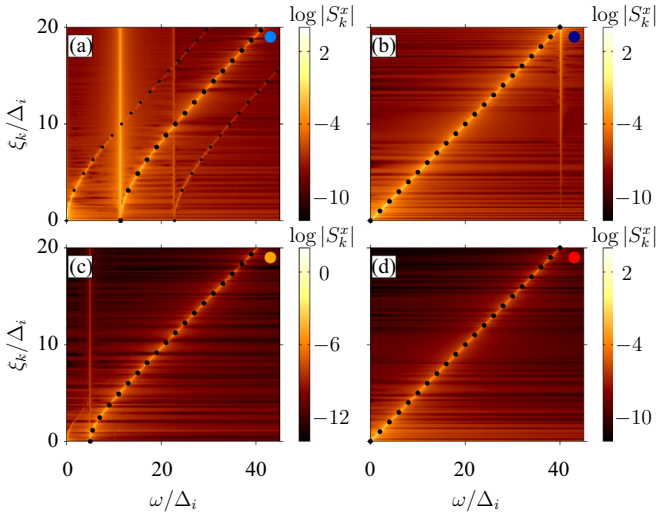

FIG. 4. Fourier transforms of the x component of the pseudospin textures for the four possible dynamical phases in the constant DOS model: non-ZOPA persistent oscillation (a), ZOPA persistent oscillation (b), damped oscillations (c), and overdamped (d). For each panel, the used quench parameters (δ) corresponds to the matching full colored circles in Fig. 1 and the colors of the dynamics in Fig. 2. For all panels $\lambda_f/\lambda_i > 0$ except for (b), which corresponds to the CQ. In this case, the synchronization phenomenon appears as a vertical intensity line close to the upper edge, $\omega = 40\Delta_i$. The FTs were computed considering a time window $t\,\Delta_i \in [0, 100]$ [62]. The large black dots represent the self-consistent Larmor frequency in each case (see text). Some replicas are indicated with small black dots in panel (a).

Figure 4(c) shows the same information in the damped oscillatory regime for the flat-DOS case. Each pseudospin oscillates with an effective Larmor frequency $2\sqrt{\xi_{\boldsymbol{k}}^2 + \Delta_\infty^2}$ (black dots) which introduces dephasing giving rise to damped oscillations in $\Delta(t)$ [cf. Fig. 2(a)]. The vertical line at $\omega = 2\Delta_\infty$ is due to the finite time window in which the FT is performed. In the long time limit, its spectral weight vanishes, indicating the absence of persistent oscillations.

In the case of the graphene-like DOS, a damped oscillatory regime is absent and a synchronized ZOPA phase appears for positive δ. The Fourier transform of the x component of the pseudospin textures dynamics is shown in Fig. 5(c). Since this phase is gapless (ZOPA) the line of black dots extrapolates to the origin. Also a vertical feature at ω_D can be seen, indicating the system syncronizes at the Dirac-Higgs frequency.

By decreasing enough the final coupling, the system enters into the gapless overdamped phase, where each pseudospin oscillates with its own bare Larmor frequency $2\xi_{\boldsymbol{k}}$ with the dispersion again extrapolating to the origin [see black dots in Figs. 4(d) and 5(d)].

In the case of the CQ [Figs. 4(b) and 5(b)], the pseudospin-resolved FT shows both the individual bare Larmor frequency, $2\xi_{\boldsymbol{k}}$ and a vertical feature in the upper edge corresponding to the upper-edge Higgs mode. The frequency is $\omega_u \approx W = 40\Delta_i$ and the intensity increase with $\xi_{\boldsymbol{k}}$ indicating that high-energy pseudospins participate with larger amplitude. This shows that the upper-edge singularity of the DOS is enough to trigger the SHP (appearing as a vertical feature) with frequency $\omega_u \simeq W$ provided that the appropriate protocol, i.e., the CQ, is used. Thus, the $1/\sqrt{\omega - 2\bar{\Delta}}$ divergence present at the lower edge of the DOS is not a prerequisite to stabilize Higgs modes. On the other hand, having a singularity at the upper edge, as is the case for the DOS of a one-dimensional system, enhances the corresponding SHP [see Fig. 9 in Sec. III C].

No feature associated with the Van Hove–Higgs mode ω_V can be seen in Fig. 5(b), since the numerical analysis has been performed on a time window larger than its coherence time in order to have high-frequency resolution. Here again the ZOPA manifests as a gapless linear dispersion of single-particle excitations, $\Omega_L(\boldsymbol{k}) = 2\xi_{\boldsymbol{k}}$ (black dots).

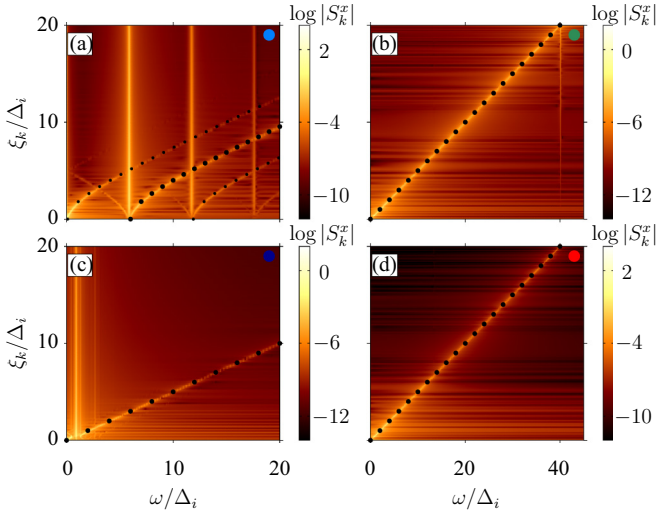

FIG. 5. Same as Fig. 4 for a graphene-like DOS with corresponding dynamics in Fig. 3. Here the dynamical phases are non-ZOPA persistent oscillation (a), ZOPA persistent oscillation for CQ (b), ZOPA persistent oscillation for non-CQ (c), and overdamped (d).

B. Linear response and participation ratio analysis

A striking characteristic of the phase diagram of the Dirac system shown in Fig. 1(b) is the absence of the damped regime. Linear response theory gives a first hint on this behavior. The susceptibility to an external perturbation which couples linearly with the pairing field reads [16,64,70]

$$\chi_{\Delta,\Delta}(\omega) \equiv \frac{\chi^0_{\Delta,\Delta}(\omega)}{1 - 2\lambda_i \chi^0_{\Delta,\Delta}(\omega)}, \tag{9}$$

where

$$\chi^0_{\Delta,\Delta}(\omega) = -\sum_k \frac{\xi_k^2}{\sqrt{\Delta^2 + \xi_k^2}\left[(\omega - i\delta)^2 - 4\left(\Delta^2 + \xi_k^2\right)\right]} \tag{10}$$

is the bare susceptibility and we assume an equilibrium gap parameter Δ. We can convert the sum to an integral by inserting the corresponding DOS. In Fig. 6 we show the imaginary part of $\chi_{\Delta,\Delta}(\omega)$ for the flat DOS with dashed curve while the full curve corresponds to the case of the graphene-like

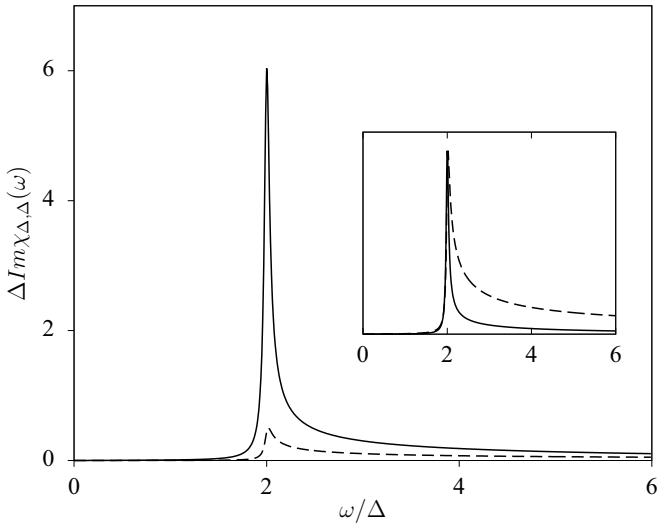

FIG. 6. Imaginary part of the interacting susceptibility for the flat DOS (dashed curve) and the graphene-like DOS (full curve). In the inset, we show the same plot but scaled to bring the maximum of the two peaks together to highlight the difference in their widths.

DOS. The peak at 2Δ corresponds to the lower-edge Higgs oscillation, which is damped in linear response. In the case of a flat DOS, it has a very small oscillator strength compared to the Dirac model, as witnessed by the difference in the peak heights. The inset shows that by rescaling the intensities, the Dirac system shows a narrower resonance, indicating a slower decay. Both factors favor synchronization for the Dirac system in an out-of-equilibrium situation. Similar changes in the power law of oscillations for a nonconstant DOS were obtained in Ref. [72–74].

Notice that, taken literally, the linear response computation would imply a damped response for an infinitesimal excitation even in the Dirac case, while we find that there is no such dynamical phase. One should keep in mind that linear response assumes an infinitesimal damping from the outset, while the exact solution has no damping. Therefore, although the linear response result is suggestive, the final result of the two computations may differ.

To further characterize the dynamics in the synchronized phase for both models, we go back to the Fourier transform of the x component of the pseudospins in Figs. 4(a) and 5(a). In Fig. 7 we plot the modulus of the Fourier component at the frequency of the synchronized mode, $|S_k(\omega = \omega_l)|$, as a function of $\xi_{\mathbf{k}}$. This yields the participation ratio of quasiparticles to the synchronization. We see that the curve is very similar for both models, but the graphene-like DOS avoids quasiparticles close to the Fermi level, which do not participate in the synchronization. Indeed, an analysis of the equation of motion reveals that, in the pseudospin language, the torque at the Fermi level vanishes. Thus, for the flat-DOS case, there is a range of quasiparticles that have a small contribution to synchronization but can contribute significantly to decoherence, while in the graphene-like DOS those quasiparticles are removed. This allows to rationalize why the graphene-like DOS is more prone to synchronization. To confirm this interpretation, in the next section, we analyze modified DOS models.

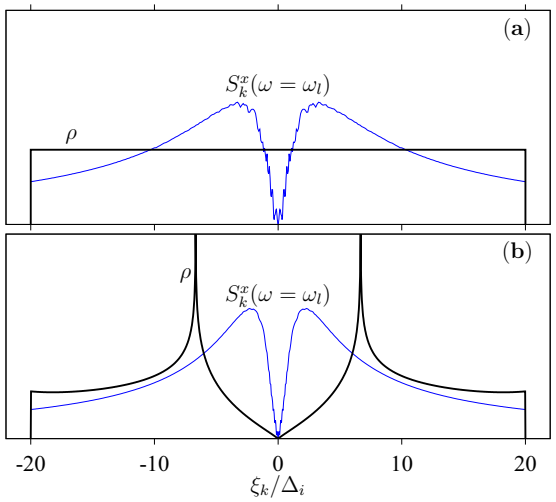

FIG. 7. Participation ratio of quasiparticles to the synchronized phase for the flat-DOS (a) and the graphene-like DOS case (b). We show the modulus of the Fourier transform of the x component of the pseudospins at the frequency of the synchronized mode as a function of the bare quasiparticle energy (blue). The black curves are the corresponding DOS. We use the same parameters as in Fig. 4(a) and Fig. 5(a). For the flat-DOS case in (a), $\delta = -2$ and $\omega_l = 2\bar{\Delta} = 11.31\Delta_i$ while for a graphene-like DOS case in (b) we are considering $\delta = -0.42$ leading to a Higgs mode frequency $\omega_l = 2\bar{\Delta} = 5.86\Delta_i$.

C. Dynamical phase diagram for other models

To further illustrate the effect of the DOS on the phase diagram, we show in Fig. 8 the dynamical phase diagram for four different models. Figure 8(b) is the flat-DOS model for reference. Figure 8(d) mimics the Dirac system by introducing a linear indentation of the DOS around the Fermi

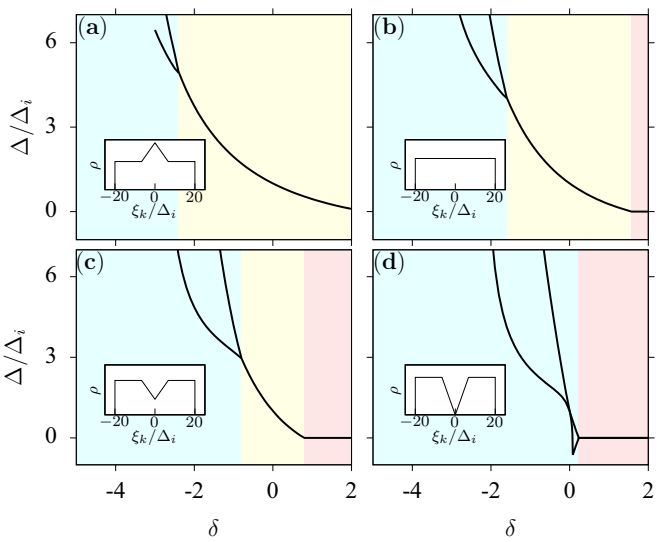

FIG. 8. Dynamical phase diagrams for four different models. In each panel the inset shows the corresponding DOS. Background color indicates synchronized regime (light blue), damped oscillations (yellow), and overdamped gapless regime (red). Full lines are gap parameters defined as in Fig. 1.

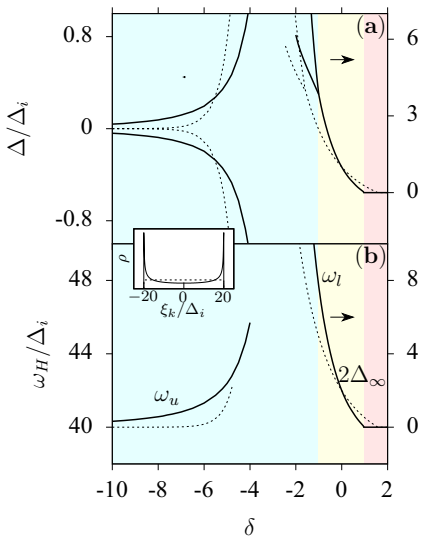

FIG. 9. Dynamical phase diagrams for a DOS corresponding to a one-dimensional tight-binding model with nearest neighbor hopping, as shown in the inset (full lines). Background colors have the same meaning as in Fig. 1 and Fig. 8. Dashed lines show gap parameters and frequencies for the flat-DOS case as a reference.

level, as shown in the inset. Here a Van Hove singularity is absent, and we see that the phase diagram is very similar to the graphene-like DOS, i.e., without the damped phase. Figure 8(c) interpolates between these two models and shows a narrow region with a damped phase (yellow). Figure 8(a) illustrates the case in which there is an excess of DOS at the origin, and we see that the damped region broadens. We conclude that quasiparticles near the Fermi level favor decoherence and disfavor the synchronized phase.

For completeness, we show in Fig. 9 the phase diagram for the DOS corresponding to a one-dimensional tight-binding model with nearest-neighbor hopping which has square root singularities at the band edges (see inset). In this case, the rightmost part of the phase diagram (non CQ) is qualitatively similar to the flat-DOS case (shown with dashed lines) as the central part of the DOS is very similar to a flat DOS. On the other hand, for CQ one notices, in Fig. 9(b), that the upper-edge Higgs frequency converges to the bandwidth energy $W = 40\Delta_i$ as $\delta \to -\infty$ ($\lambda_f \to 0^-$) as a power law, while the behavior for the flat-DOS case is exponential. The same can be said for the amplitude of the oscillation in Fig. 9(a). The behavior is analogous to the one of an impurity state creating a bound state in a tight-binding model, where the bound state energy is exponentially small if the DOS has an edge and behaves as a power law for a one-dimensional system [75].

IV. CONCLUSIONS

We have shown that different synchronized Higgs phases can be excited in a BCS system by choosing an appropriate quench protocol. For a given system, the frequency of the mode is determined by singularities in the DOS with small corrections due to quasiparticle interactions. The previously known lower-edge Higgs mode appears at the same frequency of a singularity in the equilibrium particle-particle response. The upper-edge SHP is reminiscent of antibound states appearing in the equilibrium pairing response of repulsive systems. However, at equilibrium the mode is not present in particle-hole symmetric situations [76], while here the mode is stabilized in an out-of-equilibrium setting. Thus, generalized Higgs modes do not appear to have always an equilibrium counterpart.

Our findings provide an innovative interpretation to the Higgs mode dynamics, which appear as synchronized quasiparticles oscillations nucleated by DOS singularities. This, in turns, implies that any spectral singularity can give rise to Higgs-mode like oscillations given a suitable quench.

One possibility to create singularities in the DOS is through confinement in a nanoscale wire. A detailed study [72] have revealed differences in the oscillatory dynamics depending on the shape of the local DOS. Also, confinement in ultracold atoms leads to similar effects [73,74].

The observation of the previously reported lower-edge SHP in real superconductors is hindered by its decay in other excitations and its weak coupling to light [26,27,29,63]. Furthermore, signatures of Higgs dynamics in pump and probe experiments [20,21,77] cannot be clearly distinguished from Raman modes [78] with similar frequencies, but different character. The experimental detection of other Higgs modes presented here will probably encounter similar difficulties in solid state systems, as our picture is based on the BCS model, whose integrable nature does not account for thermalization.

A proper understanding of the generalized Higgs dynamics, as well as the possible relation with the equilibrium characteristic of the SSB phase, may be obtained by direct observation in Fermi superfluids of cold atoms. Indeed, recent improvements in the control and observation of ultracold atoms in optical lattices [79,80] allowed the study of both equilibrium and transport properties of Fermi systems on the lattice [81–84], paving the way to the realization of the generalized Higgs dynamics described here. In particular, an artificial graphene-like lattice with tunable interactions has been realized [85,86]. Another route is to use cold atoms in an optical cavity, which has recently been proposed as a BCS simulator [87].

Interestingly, the search for more than one Higgs boson is a subject of intense search also in high-energy scattering experiments [88]. This kind of probes, however, are more akin to equilibrium responses in condensed matter. Instead, the strongly out-of-equilibrium physics investigated here may find parallels in the electroweak transition of relevance for early universe cosmology and baryogenesis [89].

ACKNOWLEDGMENTS

We thank C. Balseiro, G. Usaj, G. Seibold, L. Benfatto, C. Castellani, J. Sofo, and M. Papinutto for useful discussions. We acknowledge financial support from the Italian Ministry for University and Research through PRIN Projects No. 2017Z8TS5B and No. 20207ZXT4Z. H.P.O.C. is supported by the Marie Skłodowska-Curie individual fellowship grant agreement, SUPERDYN No. 893743. This work is supported by the Deutsche Forschungsgemeinschaft (DFG, German Research Foundation) under Germany's Excellence

Strategy EXC2181/1-390900948 (the Heidelberg STRUCTURES Excellence Cluster).

APPENDIX: LAX ROOTS ANALYSIS

Because of the integrability of the BCS model, the different dynamical phases can be obtained by analyzing the integrals of motion. For this purpose, it is useful to define the so-called Lax vector [60,90,91] defined as a function of an auxiliary complex parameter y,

$$\boldsymbol{L}(y) = \boldsymbol{z} + \lambda_f \sum_{\boldsymbol{k}} \frac{\boldsymbol{S_k}}{y - \xi_{\boldsymbol{k}}}, \tag{A1}$$

where $\boldsymbol{z}$ is a unit vector along the z direction, and $\boldsymbol{S_k}$ is the pseudospin texture before the quench. The square of the Lax vector is a conserved quantity under time evolution with the BCS Hamiltonian. Therefore, the complex roots of such vector (in the following Lax roots) are also conserved. Since the square of the Lax vector is nonnegative, all roots are complex-conjugated pairs. Furthermore, due to the electron-hole symmetry of the problem, it is easy to show that if the initial texture is particle-hole symmetric then if y is a Lax root $-y$ is also a root. We choose the initial superconducting order parameter, Δ, to be real. Also, this property is preserved at all times due to particle-hole symmetry.

As previously discussed [90,91], Lax roots provide information on the frequency spectrum in the Fourier transform of $\Delta(t)$ after a quench. Starting from the equilibrium pseudospin texture, a dense distribution of Lax roots appears along the real axis which, in the thermodynamic limit, define the continuous part of the spectrum. For $t \to \infty$ this contribution vanishes in the Fourier transform of $\Delta(t)$ and only isolated pairs of complex-conjugated Lax roots (bound states) contribute corresponding to persistent oscillations. It has been shown [90,91] that the number of discrete frequencies k in the Fourier transform of $\Delta(t)$ is equal to $m-1$. Here m is the number of isolated pairs of complex-conjugated Lax roots. Thus, $\Delta(t)$ shows persistent oscillations at long times with k different frequencies if $m > 1$ while $\Delta(t)$ converges to a constant value ($\Delta(t) \to \Delta_\infty$) if $m = 1$.

To complement the numerical results, we constructed the Lax vector and computed its roots using the equilibrium pseudospin texture for λ_i as the initial condition. For non-critical quenches ($\lambda_f/\lambda_i > 0$) the Lax analysis was done in Refs. [60,90,91] and the possible isolated pairs of Lax roots are always purely imaginary: (1) In the synchronized regime, there are two pairs of isolated roots ($m = 2$) namely, $y = \pm iu_1$ and $y = \pm iu_2$ that give information on the amplitude of persistent oscillation as $\Delta_\pm = (u_1 \pm u_2)\Delta_i$. In this case, $\Delta(t)$ shows only one fundamental frequency ($k = m - 1 = 1$) corresponding to the lower edge Higgs mode $2\bar{\Delta}$. (2) In the damped phase there is only one isolated pair of Lax roots ($m = 1$) namely, $y = \pm i\Delta_\infty$ indicating there are not persistent oscillations ($k = m - 1 = 0$) but damped. (3) In the over-damped regime, the latter pair of roots collapse to the origin ($\Delta_\infty = 0$) so no isolated roots are present ($m = 0$).

We now extend these results to the critical quench (CQ, $\lambda_f/\lambda_i < 0$). In this case, the Lax roots are complex numbers with a *finite* real part, giving precise information not only on the amplitude but also the oscillation frequency of $\Delta(t)$. Both in the case of the constant and in that of the graphene like-DOS, the roots can be written as $y = \pm(u_r \pm iu_i)$ with the real part providing information on the upper-edge Higgs mode frequency, $\omega_u = 2u_r$ and the imaginary part yielding the oscillation amplitude $\Delta_\pm = \pm 2u_i$.

For the graphene-like DOS and $\lambda_f/\lambda_i > 0$, there is a regime where $2\bar{\Delta} \neq 0$ for which the isolated Lax roots are purely imaginary, mimicking the non-ZOPA synchronized phase of the constant DOS model. Still in the synchronized regime, where the Dirac-Higgs mode emerges, the isolated Lax roots acquire a finite real part defining the mode frequency as $\omega_D = 2u_r$ and the amplitudes of oscillations $\Delta_\pm = \pm 2u_i$.

[1] Y. Nambu and G. Jona-Lasinio, Dynamical model of elementary particles based on an analogy with superconductivity. I, Phys. Rev. **122**, 345 (1961).

[2] S. Sachdev, *Quantum Phase Transitions* (Cambridge University Press, Cambridge, 2011), pp. 1–517.

[3] C. Di Castro and R. Raimondi, *Statistical Mechanics and Applications in Condensed Matter* (Cambridge University Press, Cambridge, 2015).

[4] H. Nishimori and G. Ortiz, *Elements of Phase Transitions and Critical Phenomena, Oxford Graduate Texts* (Oxford University Press, Oxford, 2011).

[5] P. W. Anderson, Plasmons, gauge invariance, and mass, Phys. Rev. **130**, 439 (1963).

[6] F. Englert and R. Brout, Broken Symmetry and the Mass of Gauge Vector Mesons, Phys. Rev. Lett. **13**, 321 (1964).

[7] P. W. Higgs, Broken Symmetries and the Masses of Gauge Bosons, Phys. Rev. Lett. **13**, 508 (1964).

[8] G. S. Guralnik, C. R. Hagen, and T. W. B. Kibble, Global Conservation Laws and Massless Particles, Phys. Rev. Lett. **13**, 585 (1964).

[9] T. W. B. Kibble, Englert-Brout-Higgs-Guralnik-Hagen-Kibble mechanism, Scholarpedia **4**, 6441 (2009).

[10] L. Álvarez-Gaumé and J. Ellis, Eyes on a prize particle, Nat. Phys. **7**, 2 (2011).

[11] L. N. Cooper, Bound electron pairs in a degenerate Fermi gas, Phys. Rev. **104**, 1189 (1956).

[12] J. Bardeen, L. N. Cooper, and J. R. Schrieffer, Theory of superconductivity, Phys. Rev. **108**, 1175 (1957).

[13] R. Sooryakumar and M. V. Klein, Raman Scattering by Superconducting-Gap Excitations and Their Coupling to Charge-Density Waves, Phys. Rev. Lett. **45**, 660 (1980).

[14] C. A. Balseiro and L. M. Falicov, Phonon Raman Scattering in Superconductors, Phys. Rev. Lett. **45**, 662 (1980).

[15] P. B. Littlewood and C. M. Varma, Gauge-Invariant Theory of the Dynamical Interaction of Charge Density Waves and Superconductivity, Phys. Rev. Lett. **47**, 811 (1981).

[16] T. Cea and L. Benfatto, Nature and Raman signatures of the Higgs amplitude mode in the coexisting superconducting and charge-density-wave state, Phys. Rev. B **90**, 224515 (2014).

[17] R. Grasset, T. Cea, Y. Gallais, M. Cazayous, A. Sacuto, L. Cario, L. Benfatto, and M.-A. Méasson, Higgs-mode radiance and charge-density-wave order in 2H-$NbSe_2$, Phys. Rev. B **97**, 094502 (2018).

[18] C. Rüegg, B. Normand, M. Matsumoto, A. Furrer, D. F. McMorrow, K. W. Krämer, H. U. Güdel, S. N. Gvasaliya, H. Mutka, and M. Boehm, Quantum Magnets under Pressure: Controlling Elementary Excitations in $TlCuCl_3$, Phys. Rev. Lett. **100**, 205701 (2008).

[19] W. P. Halperin and E. Varoquaux, in *Helium Three, Modern Problems in Condensed Matter Sciences*, edited by W. P. Halperin and L. P. Pitaevskii (Elsevier, Amsterdam, 1990), Vol. 26, pp. 353–522.

[20] R. Matsunaga, Y. I. Hamada, K. Makise, Y. Uzawa, H. Terai, Z. Wang, and R. Shimano, Higgs Amplitude Mode in the BCS Superconductors $Nb_{1-x}Ti_xN$ Induced by Terahertz Pulse Excitation, Phys. Rev. Lett. **111**, 057002 (2013).

[21] R. Matsunaga, N. Tsuji, H. Fujita, A. Sugioka, K. Makise, Y. Uzawa, H. Terai, Z. Wang, H. Aoki, and R. Shimano, Light-induced collective pseudospin precession resonating with Higgs mode in a superconductor, Science **345**, 1145 (2014).

[22] D. Sherman, U. S. Pracht, B. Gorshunov, S. Poran, J. Jesudasan, M. Chand, P. Raychaudhuri, M. Swanson, N. Trivedi, A. Auerbach *et al.*, The Higgs mode in disordered superconductors close to a quantum phase transition, Nat. Phys. **11**, 188 (2015).

[23] K. Katsumi, N. Tsuji, Y. I. Hamada, R. Matsunaga, J. Schneeloch, R. D. Zhong, G. D. Gu, H. Aoki, Y. Gallais, and R. Shimano, Higgs Mode in the d-Wave Superconductor $Bi_2Sr_2CaCu_2O_{8+x}$ Driven by an Intense Terahertz Pulse, Phys. Rev. Lett. **120**, 117001 (2018).

[24] H. Chu, M.-J. Kim, K. Katsumi, S. Kovalev, R. D. Dawson, L. Schwarz, N. Yoshikawa, G. Kim, D. Putzky, Z. Z. Li *et al.*, Phase-resolved Higgs response in superconducting cuprates, Nat. Commun. **11**, 1793 (2020).

[25] R. Shimano and N. Tsuji, Higgs mode in superconductors, Annu. Rev. Condens. Matter Phys. **11**, 103 (2020).

[26] D. Podolsky, A. Auerbach, and D. P. Arovas, Visibility of the amplitude (Higgs) mode in condensed matter, Phys. Rev. B **84**, 174522 (2011).

[27] R. G. Scott, F. Dalfovo, L. P. Pitaevskii, and S. Stringari, Rapid ramps across the BEC-BCS crossover: A route to measuring the superfluid gap, Phys. Rev. A **86**, 053604 (2012).

[28] Y. Barlas and C. M. Varma, Amplitude or Higgs modes in d-wave superconductors, Phys. Rev. B **87**, 054503 (2013).

[29] T. Cea, C. Castellani, G. Seibold, and L. Benfatto, Nonrelativistic Dynamics of the Amplitude (Higgs) Mode in Superconductors, Phys. Rev. Lett. **115**, 157002 (2015).

[30] T. Cea, C. Castellani, and L. Benfatto, Nonlinear optical effects and third-harmonic generation in superconductors: Cooper pairs versus Higgs mode contribution, Phys. Rev. B **93**, 180507(R) (2016).

[31] S. Gazit, D. Podolsky, and A. Auerbach, Fate of the Higgs Mode near Quantum Criticality, Phys. Rev. Lett. **110**, 140401 (2013).

[32] B. Liu, H. Zhai, and S. Zhang, Evolution of the Higgs mode in a fermion superfluid with tunable interactions, Phys. Rev. A **93**, 033641 (2016).

[33] X. Han, B. Liu, and J. Hu, Observability of Higgs mode in a system without Lorentz invariance, Phys. Rev. A **94**, 033608 (2016).

[34] M. Silaev, Nonlinear electromagnetic response and Higgs-mode excitation in BCS superconductors with impurities, Phys. Rev. B **99**, 224511 (2019).

[35] Y. Murotani and R. Shimano, Nonlinear optical response of collective modes in multiband superconductors assisted by nonmagnetic impurities, Phys. Rev. B **99**, 224510 (2019).

[36] U. Bissbort, S. Götze, Y. Li, J. Heinze, J. S. Krauser, M. Weinberg, C. Becker, K. Sengstock, and W. Hofstetter, Detecting the Amplitude Mode of Strongly Interacting Lattice Bosons by Bragg Scattering, Phys. Rev. Lett. **106**, 205303 (2011).

[37] M. Endres, T. Fukuhara, D. Pekker, M. Cheneau, P. Schauß, C. Gross, E. Demler, S. Kuhr, and I. Bloch, The 'Higgs' amplitude mode at the two-dimensional superfluid/Mott insulator transition, Nature (London) **487**, 454 (2012).

[38] T. M. Hoang, H. M. Bharath, M. J. Boguslawski, M. Anquez, B. A. Robbins, and M. S. Chapman, Adiabatic quenches and characterization of amplitude excitations in a continuous quantum phase transition, Proc. Natl. Acad. Sci. USA **113**, 9475 (2016).

[39] J. Léonard, A. Morales, P. Zupancic, T. Donner, and T. Esslinger, Monitoring and manipulating Higgs and Goldstone modes in a supersolid quantum gas, Science **358**, 1415 (2017).

[40] A. Behrle, T. Harrison, J. Kombe, K. Gao, M. Link, J. S. Bernier, C. Kollath, and M. Köhl, Higgs mode in a strongly interacting fermionic superfluid, Nat. Phys. **14**, 781 (2018).

[41] J. Bjerlin, S. M. Reimann, and G. M. Bruun, Few-Body Precursor of the Higgs Mode in a Fermi Gas, Phys. Rev. Lett. **116**, 155302 (2016).

[42] L. Bayha, M. Holten, R. Klemt, K. Subramanian, J. Bjerlin, S. M. Reimann, G. M. Bruun, P. M. Preiss, and S. Jochim, Observing the emergence of a quantum phase transition shell by shell, Nature (London) **587**, 583 (2020).

[43] M. Heyl, Dynamical quantum phase transitions: A review, Rep. Prog. Phys. **81**, 054001 (2018).

[44] M. Eckstein, M. Kollar, and P. Werner, Thermalization after an Interaction Quench in the Hubbard Model, Phys. Rev. Lett. **103**, 056403 (2009).

[45] J. P. Garrahan and I. Lesanovsky, Thermodynamics of Quantum Jump Trajectories, Phys. Rev. Lett. **104**, 160601 (2010).

[46] S. Diehl, A. Tomadin, A. Micheli, R. Fazio, and P. Zoller, Dynamical Phase Transitions and Instabilities in Open Atomic Many-Body Systems, Phys. Rev. Lett. **105**, 015702 (2010).

[47] M. Schiró and M. Fabrizio, Time-Dependent Mean Field Theory for Quench Dynamics in Correlated Electron Systems, Phys. Rev. Lett. **105**, 076401 (2010).

[48] B. Sciolla and G. Biroli, Quantum Quenches and Off-Equilibrium Dynamical Transition in the Infinite-Dimensional Bose-Hubbard Model, Phys. Rev. Lett. **105**, 220401 (2010).

[49] G. Mazza, From sudden quench to adiabatic dynamics in the attractive Hubbard model, Phys. Rev. B **96**, 205110 (2017).

[50] M. Heyl, A. Polkovnikov, and S. Kehrein, Dynamical Quantum Phase Transitions in the Transverse-Field Ising Model, Phys. Rev. Lett. **110**, 135704 (2013).

[51] M. Heyl, Scaling and Universality at Dynamical Quantum Phase Transitions, Phys. Rev. Lett. **115**, 140602 (2015).

[52] P. Jurcevic, H. Shen, P. Hauke, C. Maier, T. Brydges, C. Hempel, B. P. Lanyon, M. Heyl, R. Blatt, and C. F. Roos, Direct Observation of Dynamical Quantum Phase Transitions in an Interacting Many-Body System, Phys. Rev. Lett. **119**, 080501 (2017).

[53] J. Zhang, G. Pagano, P. W. Hess, A. Kyprianidis, P. Becker, H. Kaplan, A. V. Gorshkov, Z. X. Gong, and C. Monroe, Observation of a many-body dynamical phase transition with a 53-qubit quantum simulator, Nature (London) **551**, 601 (2017).

[54] B. Žunkovič, M. Heyl, M. Knap, and A. Silva, Dynamical Quantum Phase Transitions in Spin Chains with Long-Range Interactions: Merging Different Concepts of Nonequilibrium Criticality, Phys. Rev. Lett. **120**, 130601 (2018).

[55] J. C. Halimeh and V. Zauner-Stauber, Dynamical phase diagram of quantum spin chains with long-range interactions, Phys. Rev. B **96**, 134427 (2017).

[56] J. C. Halimeh, V. Zauner-Stauber, I. P. McCulloch, I. de Vega, U. Schollwöck, and M. Kastner, Prethermalization and persistent order in the absence of a thermal phase transition, Phys. Rev. B **95**, 024302 (2017).

[57] N. Defenu, T. Enss, and J. C. Halimeh, Dynamical criticality and domain-wall coupling in long-range Hamiltonians, Phys. Rev. B **100**, 014434 (2019).

[58] P. Uhrich, N. Defenu, R. Jafari, and J. C. Halimeh, Out-of-equilibrium phase diagram of long-range superconductors, Phys. Rev. B **101**, 245148 (2020).

[59] R. A. Barankov, L. S. Levitov, and B. Z. Spivak, Collective Rabi Oscillations and Solitons in a Time-Dependent BCS Pairing Problem, Phys. Rev. Lett. **93**, 160401 (2004).

[60] R. A. Barankov and L. S. Levitov, Synchronization in the BCS Pairing Dynamics as a Critical Phenomenon, Phys. Rev. Lett. **96**, 230403 (2006).

[61] P. W. Anderson, Random-Phase Approximation in the Theory of Superconductivity, Phys. Rev. **112**, 1900 (1958).

[62] Data available at https://doi.org/10.5281/zenodo.6560359.

[63] H. P. Ojeda Collado, G. Usaj, J. Lorenzana, and C. A. Balseiro, Fate of dynamical phases of a BCS superconductor beyond the dissipationless regime, Phys. Rev. B **99**, 174509 (2019).

[64] H. P. Ojeda Collado, J. Lorenzana, G. Usaj, and C. A. Balseiro, Population inversion and dynamical phase transitions in a driven superconductor, Phys. Rev. B **98**, 214519 (2018).

[65] H. P. Ojeda Collado, G. Usaj, C. A. Balseiro, D. H. Zanette, and J. Lorenzana, Emergent parametric resonances and time-crystal phases in driven Bardeen-Cooper-Schrieffer systems, Phys. Rev. Res. **3**, L042023 (2021).

[66] H. P. Ojeda Collado, G. Usaj, C. A. Balseiro, D. H. Zanette, and J. Lorenzana, Dynamical phase transitions in periodically driven Bardeen-Cooper-Schrieffer systems, arXiv:2210.15693.

[67] M. Mootz, J. Wang, and I. E. Perakis, Lightwave terahertz quantum manipulation of nonequilibrium superconductor phases and their collective modes, Phys. Rev. B **102**, 054517 (2020).

[68] Y.-Z. Chou, Y. Liao, and M. S. Foster, Twisting Anderson pseudospins with light: Quench dynamics in terahertz-pumped BCS superconductors, Phys. Rev. B **95**, 104507 (2017).

[69] G. Seibold and J. Lorenzana, Nonequilibrium dynamics from BCS to the bosonic limit, Phys. Rev. B **102**, 144502 (2020).

[70] A. F. Volkov and Sh. M. Kogan, Collisionless relaxation of the energy gap in superconductors, Zh. Eksp. Teor. Fiz. **65**, 2038 (1973) [Sov. Phys. JETP **38**, 1018 (1974)].

[71] G. Homann, J. G. Cosme, and L. Mathey, Higgs time crystal in a high-T_c superconductor, Phys. Rev. Res. **2**, 043214 (2020).

[72] M. Zachmann, M. D. Croitoru, A. Vagov, V. M. Axt, T. Papenkort and T. Kuhn, Ultrafast terahertz-field-induced dynamics of superconducting bulk and quasi-1D samples, New J. Phys. **15**, 055016 (2013).

[73] S. Hannibal, P. Kettmann, M. D. Croitoru, V. M. Axt, and T. Kuhn, Dynamical vanishing of the order parameter in a confined Bardeen-Cooper-Schrieffer Fermi gas after an interaction quench, Phys. Rev. A **97**, 013619 (2018).

[74] S. Hannibal, P. Kettmann, M. D. Croitoru, V. M. Axt, and T. Kuhn, Persistent oscillations of the order parameter and interaction quench phase diagram for a confined Bardeen-Cooper-Schrieffer Fermi gas, Phys. Rev. A **98**, 053605 (2018).

[75] E. N. Economou, *Green's Functions in Quantum Physics* (Springer, Berlin, 2006).

[76] G. Seibold, F. Becca, and J. Lorenzana, Theory of Antibound States in Partially Filled Narrow Band Systems, Phys. Rev. Lett. **100**, 016405 (2008).

[77] M. Buzzi, G. Jotzu, A. Cavalleri, J. I. Cirac, E. A. Demler, B. I. Halperin, M. D. Lukin, T. Shi, Y. Wang, and D. Podolsky, Higgs-Mediated Optical Amplification in a Nonequilibrium Superconductor, Phys. Rev. X **11**, 011055 (2021).

[78] B. Mansart, J. Lorenzana, a. Mann, a. Odeh, M. Scarongella, M. Chergui, and F. Carbone, Coupling of a high-energy excitation to superconducting quasiparticles in a cuprate from coherent charge fluctuation spectroscopy, Proc. Natl. Acad. Sci. USA **110**, 4539 (2013).

[79] N. Goldman, J. C. Budich, and P. Zoller, Topological quantum matter with ultracold gases in optical lattices, Nat. Phys. **12**, 639 (2016).

[80] C. Gross and I. Bloch, Quantum simulations with ultracold atoms in optical lattices, Science **357**, 995 (2017).

[81] A. Mazurenko, C. S. Chiu, G. Ji, M. F. Parsons, M. Kanász-Nagy, R. Schmidt, F. Grusdt, E. Demler, D. Greif, and M. Greiner, A cold-atom Fermi-Hubbard antiferromagnet, Nature (London) **545**, 462 (2017).

[82] J. Koepsell, J. Vijayan, P. Sompet, F. Grusdt, T. A. Hilker, E. Demler, G. Salomon, I. Bloch, and C. Gross, Imaging magnetic polarons in the doped Fermi-Hubbard model, Nature (London) **572**, 358 (2019).

[83] P. T. Brown, D. Mitra, E. Guardado-Sanchez, R. Nourafkan, A. Reymbaut, C.-D. Hébert, S. Bergeron, A. M. S. Tremblay, J. Kokalj, D. A. Huse *et al.*, Bad metallic transport in a cold atom Fermi-Hubbard system, Science **363**, 379 (2019).

[84] M. A. Nichols, L. W. Cheuk, M. Okan, T. R. Hartke, E. Mendez, T. Senthil, E. Khatami, H. Zhang, and M. W. Zwierlein, Spin transport in a Mott insulator of ultracold fermions, Science **363**, 383 (2019).

[85] T. Uehlinger, G. Jotzu, M. Messer, D. Greif, W. Hofstetter, U. Bissbort, and T. Esslinger, Artificial Graphene with Tunable Interactions, Phys. Rev. Lett. **111**, 185307 (2013).

[86] C. D. Brown, S.-W. Chang, M. N. Schwarz, T.-H. Leung, V. Kozii, A. Avdoshkin, J. E. Moore, and D. Stamper-Kurn, Direct geometric probe of singularities in band structure, Science **377**, 1319 (2022).

[87] R. J. Lewis-Swan, D. Barberena, J. R. K. Cline, D. J. Young, J. K. Thompson, and A. M. Rey, Cavity-QED Quantum Simulator of Dynamical Phases of a Bardeen-Cooper-Schrieffer Superconductor, Phys. Rev. Lett. **126**, 173601 (2021).

[88] A. Tumasyan, W. Adam, J. W. Andrejkovic, T. Bergauer, S. Chatterjee, M. Dragicevic, A. Escalante Del Valle, R.

Frühwirth, M. Jeitler *et al.* (The CMS collaboration), Search for a heavy Higgs boson decaying into two lighter Higgs bosons in the $\tau\tau$bb final state at 13 TeV, J. High Energy Phys. 11 (2021) 057.

[89] B. Ghosh, Electroweak phase transition and some related phenomena - a brief review, Pramana **87**, 43 (2016).

[90] E. A. Yuzbashyan, O. Tsyplyatyev, and B. L. Altshuler, Relaxation and Persistent Oscillations of the Order Parameter in Fermionic Condensates, Phys. Rev. Lett. **96**, 097005 (2006).

[91] E. A. Yuzbashyan, Normal and anomalous solitons in the theory of dynamical Cooper pairing, Phys. Rev. B **78**, 184507 (2008).